THE JOURNAL OF PHYSICAL CHEMISTRY B

Article

pubs.acs.org/JPCB

Molecular Response and Cooperative Behavior during the Interactions of Melittin with a Membrane: Dissipative Quartz Crystal Microbalance Experiments and Simulations

Naiyan Lu,[‡] Kai Yang,[†] Bing Yuan,*[,†] and Yuqiang Ma*[,‡,†]

[†]Center for Soft Condensed Matter Physics and Interdisciplinary Research, Soochow University, Suzhou, 215006, P. R. China

[‡]National Laboratory of Solid State Microstructures and Department of Physics, Nanjing University, Nanjing, 210093, P. R. China

Supporting Information

ABSTRACT: The molecular-level interactions of an antimicrobial peptide melittin with supported membrane were studied by the combination of dissipative quartz crystal microbalance (QCM-D) experiments and computer simulations. We found the response behavior of lipids upon peptide adsorption greatly influence their interactions. The perturbance and reorientation of the lipid in liquid phase facilitate the insertion of melittin in a trans-membrane way, but in solid phase, asymmetrical membrane disruption happens. Apart from the lipid state, the local peptide-to-lipid ratio also affects the insertion capacity of melittin. When the local peptide number density is high, adjacent peptides can cooperatively penetrate into the membrane. This observation explains the occurrence of the conventional "carpet" mechanism.

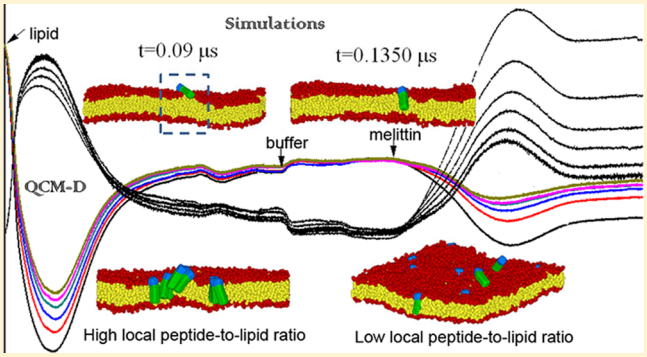

1. INTRODUCTION

The ability of antimicrobial peptides (AMPs) to lyse pathogen cell membranes makes them promising candidates for the next generation of antibiotics which are required urgently because of the increasing resistance of bacteria to conventional antibiotics.[1−3] Moreover, the lipid-active properties of these peptides, such as the pore-forming ability, make them suitable models for exploring protein−lipid interactions.[4,5] Melittin is an intensively studied antimicrobial and hemolytic peptide.[6] The biological activity of melittin on both whole bacterial cells[7,8] and model membranes[9,10] has been investigated. In the presence of membrane, melittin folds into amphiphilic α-helices, and its lipid-activity is significantly influenced by the peptide concentration and membrane properties.[6] One widely accepted model assumes that melittin binds to a membrane surface when the peptide-to-lipid ratio is below a threshold value, and induces the thinning of the bilayer, whereas at higher ratio, it inserts into and destabilize the membrane, which results in a leakage of cell components and eventually cell death (the "carpet" mechanism).[11−13] The proposed membrane disruption process includes the pore formation, mostly as toroidal pores composed of a mixture of peptides and lipid headgroups,[14,15] or membrane disintegration and/or micellization.[16] Charged components[17] and cholesterol[18,19] were found to have an important impact on the melittin membrane affinity, while the subsequent insertion step is modulated by the physicochemical properties of the membrane, including the composition,[20] curvature,[21] and homogeneity,[18,19] to name a few. Although several models[13,16] and experimental approaches[12,14,22] have been used to probe each step of this interaction, questions concerning the exact mechanism, such as the molecular details of a carpet mechanism, have not been fully answered yet.

A wide variety of biophysical techniques have been utilized to explore the antimicrobial mechanism of an AMP, including surface plasmon resonance (SPR),[23] fluorescence anisotropy measurements,[24] sum frequency generation (SFG) vibrational spectroscopy,[25] and atomic force microscopy (AFM),[22] *etc.* The dissipative quartz crystal microbalance (QCM-D) has been proved to be an attractive technique due to the real time and *in situ* measurement on the interaction between an AMP and a biomembrane and providing information of both the mass and structural changes occurring to the membrane.[3,26] Therefore, QCM-D is considered as a powerful tool to study the dynamic processes of adsorption, desorption and interfacial interactions between a peptide and a supported membrane.[22,27−29] A flow-through system is normally adopted in related experiments to mimic the natural conditions surrounding a membrane, which however would lead to a large uncertainty on the local peptide-to-lipid ratio during their interactions since the peptides are adsorbed to the surface. Due to the technical limits, detailed AMP action mechanism is hard to access by experiments alone. In this work, we combined the dissipative particle dynamics

Received: May 27, 2012
Revised: July 11, 2012
Published: July 15, 2012

   dx.doi.org/10.1021/jp305141r | *J. Phys. Chem. B* 2012, 116, 9432−9438

simulations, which have previously been performed for the characteristic studies of membrane,[30,31] with QCM-D experiments, to probe the interfacial interaction between melittin and supported lipid metrics on the molecular level. We first learned about the formation dynamics of the supported membrane through fusion of vesicles with different states of lipids and the quality of the supported lipid bilayers (SLBs) obtained, and then investigated the influence from lipid states and local peptide-to-lipid ratios on the interactions between them. In the previous work, the lipid state of the membrane has been regulated by varing lipid compositions, that is,the addition of phase-separated lipid or cholesterol,[19,32] whereas in this report, it was easily controlled by temperature, which avoids external disturbance to the system. Our results show that the lipid-activity of melittin significantly depends on the molecular responding behavior and cooperation effect of lipid and peptide, which on the other side are expected to have significant implications to the "carpet" phenomenon. The present study provides new insight into the underlying mechanism.

2. MATERIALS AND METHODS

2.1. Chemicals. 1,2-Dioleoyl-*cn*-glycero-3-phosphocholine (DOPC), 1,2-dipalmitoyl-*sn*-glycero-3-phosphocholine (DPPC), and cholesterol (Chol) were purchased from Avanti Lipids. Buffer solution [10 mM tris(hydroxymethyl)-aminomethane, 100 mM NaCl, and 2 mM $CaCl_2$] was adjusted to pH 7.5 with HCl. Melittin from the honey bee venom was purchased from Sigma and dissolved in buffer to 2 μg mL^{-1}.

2.2. Vesicle Preparation. SLB was fabricated *in situ* on the surface of QCM-D crystal with SiO_2 coating by the normal vesicle fusion method.[32] A solution of monodisperse unilamellar lipid vesicles was prepared by a conventional extrusion technique. Lipids with a designed ratio of DOPC:DPPC:Chol = 4:4:2 were first dissolved in chloroform, and then dried completely in a stream of N_2 gas. After that they were rehydrated in Tris buffer to 3.5 mg mL^{-1} lipid at 50 °C. The suspensions were extruded 21 times through a filter support (Avanti Polar Lipids) with the pore size of 100 nm. Light-scattering measurements revealed that vesicles with a typical size of ~110 ± 15 nm were obtained. The vesicle suspensions were stored at 4 °C and used within 3 days. The vesicles were diluted in buffer solution to a lipid concentration of 0.07 mg mL^{-1} for use.

2.3. QCM-D Monitoring. QCM-D measurements were performed on a Q-sense E1 instrument (Sweden). AT-cut quartz crystals with a fundamental frequency of 5 MHz and a diameter of 14 mm were used. The change of resonance frequency (Δf) and energy dissipation (ΔD) upon mass deposition were monitored simultaneously at six different overtones of the natural frequency (from 3rd to 13th, i.e., 15−65 MHz). Measurements at the natural frequency (5 MHz) were not considered since this resonance was very sensitive to bulk solution variations which could lead to unreliable output.[26] A flow-through system allowing successive application of a set of sample fluids to the sensor and the liquid flow was maintained throughout the measurement. An Ismatec peristaltic pump (Sweden) was settled to control the flow rate as 50 μL min^{-1}. The working temperature was 25 °C if not stated otherwise.

A SiO_2 coated sensor crystal was used for vesicle deposition. After each measurement, the crystal was taken out from the chamber and cleaned carefully for next use. The crystal was immersed in a 2 wt % SDS for 30 min and then rinsed with abundant distilled water. After that, the crystal was dried under a gentle stream of N_2 gas, and treated with UV/ozone for 10 min prior to being mounted inside the flow module. Distilled water was injected into the module for more than 1 h for stabilization. The distilled water was then replaced with buffer or other sample solutions as specified in the main text and a baseline was established right before the test. Multiple measurements for each condition were conducted for repeatability.

2.4. Simulation Method. Dissipative particle dynamics (DPD) is a coarse-grained computer simulation technique capable of including the hydrodynamic interactions,[33,34] and it has been extensively used to explore the interactions between lipid membrane and proteins.[35−37] In DPD simulations, each bead stands for a group of atoms or molecules. The evolution of the position and velocity of bead i, ($\vec{r}_i$, $\vec{v}_i$), obeys Newton's equation of motion:

$$\frac{d\vec{r}_i}{dt} = \vec{v}_i, \qquad \frac{d\vec{v}_i}{dt} = \frac{\vec{f}_i}{m}$$

The interaction between two beads is normally denoted as

$$\vec{F}_{ij}^{C} = a_{ij}\left(1 - \frac{r_{ij}}{r_c}\right)\vec{e}_{ij}$$

Here, a_{ij} represents the maximum repulsion interaction between beads i and j, $\vec{r}_{ij} = \vec{r}_i - \vec{r}_j$, $\vec{r}_{ij} = |\vec{r}_{ij}|$, and $\vec{e}_{ij} = \vec{r}_{ij}/r_{ij}$. Furthermore, random force and friction are applied to each pair of neighboring beads to keep the momentum locally conserved and produce the hydrodynamic effect.

The lipid molecule is modeled as a linear chain containing two hydrophilic head beads (h) and five hydrophobic tail beads (t) and with harmonic springs connecting neighboring beads (Figure 1a).[38−40] The spring constant is $k_s = 128k_BT/r_c$ and the equilibrium bond length is set to be $l_0 = 0.5r_c$ (r_c refers to the length unit in simulations). To ensure the rigidity of lipid tails, a three-body bond angle potential U_b with force constant $k_b = 5k_BT/r_c$ and the preferred angle $\varphi_0 = 0$ is applied: $U_b = k_b(1 - \cos(\varphi - \varphi_0))$. For the peptide melittin, a rigid body model is applied (Figure 1b).[31,41] Note that only some basic characters of the peptide, such as the amphiphilic surface (the negatively charged C-terminal), the two α-helical configuration with a bending angle of ~160°,[41] are concerned in the simulations while other molecular details are simplified. Additionally, water is explicitly included in the system as solvent (w). In the simulations, all physical quantities are scaled by the cutoff radius r_c, time step Δt, bead mass m, and temperature k_BT, which may roughly be mapped to the real units as $r_c \approx 0.8$ nm, and $\Delta t \approx 90$ ps.[31,36] The interaction parameters a_{ij} between beads are chosen according to their characters (i.e., hydrophobicity or hydrophilicity). These simulation parameters have been proved

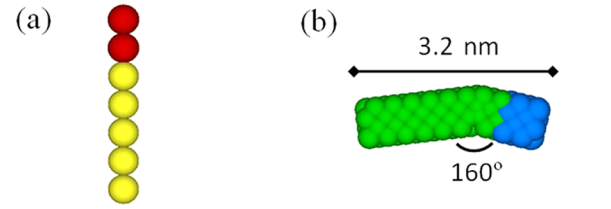

Figure 1. Coarse-grained model of lipid (a) and melittin (b). Red and yellow: the head and tail beads of a lipid; Blue and green: the hydrophilic terminal and the more hydrophobic parts of melittin.

dx.doi.org/10.1021/jp305141r | J. Phys. Chem. B 2012, 116, 9432−9438

to well reproduce the structure and mechanical character of lipid bilayers and the hydrophobic effect of the peptide.[35,37,42,43]

All simulations are performed in a simulation box of 32 nm × 32 nm × 38.4 nm with the periodic boundary conditions in three directions. A planar lipid bilayer with nearly zero surface tension is placed in the center of the simulation box (*xy* plane). To avoid the unphysical changes of lipid packing state due to the insertion of melittin, a N-varied DPD method is applied to maintain the constant surface tension of the membrane in the whole simulation process.[44,45] At the beginning of each simulation, peptides (with a number of n_p) are placed sparsely or densely on the surface of the lipid bilayer, as described in the main text in detail.

3. RESULTS AND DISCUSSION

3.1. Kinetics of Vesicle Adsorption and SLB Formation at Different Temperatures. As a basis for studying peptide-membrane interactions, we first investigate the forming process of SLBs and their quality. The most prevalent method to fabricate SLBs is vesicle fusion, which includes the vesicle adsorption and its rupture into a confluent SLB on the surface of the substrate.[22,32] In our experiments, two temperatures (25 and 50 °C) were particularly considered to explain the influence of lipid phase on SLB formation.

In a QCM-D experiment, changes in frequency (f) and dissipation (D) give information about mass and viscoelasticity of the object adsorbed on the sensor surface, respectively. Δf and ΔD refer to the raw f and D data at a certain time, normalized by the values at the start of the measurement. The decrease in frequency is proportional to the increase of mass and vice versa. The dissipation factor is evaluated from the energy loss of the sensor chip to the surrounding environment; that is, a high D suggests there is a thick and loose layer of things on the surface while a low D indicates the layer of things on the surface is rigid and compact.[3,26,46] QCM-D is an excellent approach to distinguish SLBs from adsorbed intact vesicles.[32] Figure 2 shows the QCM-D traces upon deposition of vesicles on the same SiO_2 surfaces at different temperatures, 25 and 50 °C. Note that both liquid and solid phases coexist within the vesicles at 25 °C, while at a higher temperature of 50 °C, the lipid is only in the liquid phase. Under both circumstances mentioned above, the curves show characteristic behavior of SLB formation, with an initial decrease/increase in frequency/dissipation indicating something thick and loose is adsorbing to the surface, followed by the opposite referring to an overall loss of mass from and a stiffening of the adsorbed layer on the sensor surface, after reaching a critical point. The initial mass increase stage refers to a vesicle adsorbing process, while the following decrease in mass corresponds to the rupture of vesicles and formation of SLBs, when the surface density of the adsorbed vesicles is above a threshold value. However, at a higher temperature (50 °C), the critical point shifts to a shorter time with a lower amplitude of extrema in the QCM-D responses, and after crossing over the threshold point, the system reaches the final steady state much sooner than that at 25 °C, shown as a steeper slope in the $\Delta D-\Delta f$ plot (Figure 2, inset). The ultimate shifts in both frequency and dissipation obtained at 50 °C ($\Delta f \approx -25 \pm 0.2$ Hz and $\Delta D \approx 0 \times 10^{-6}$) are consistent with the characteristic values of the formation of a high quality SLB.[22] While at the temperature of 25 °C, the deposition can cause a little larger frequency change (ca. −27 Hz) which is expected as the formation of a slightly denser (and consequently thicker) membrane with greater lipid alignment

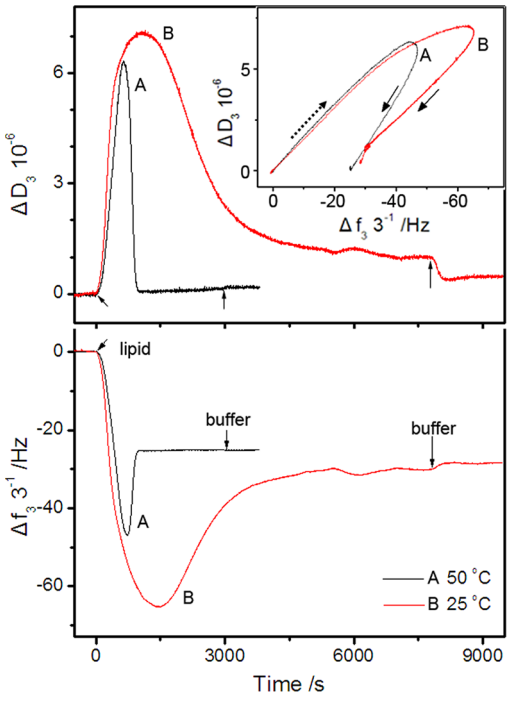

Figure 2. QCM-D traces upon deposition of vesicles on a bare SiO_2 surface at different temperatures: 25 and 50 °C. Arrows indicate the injection of certain solutions. Inset: $\Delta D-\Delta f$ plot of the same data. The dotted and solid arrows refer to the initial vesicle adsorption and the subsequent vesicle rupture dominated processes, respectively.

in the solid phase. The drop in values under buffer introduction suggests the rinsing away of the surviving and/or additional adsorbed vesicles on the surface.

A higher amplitude of extrema of Δf (referring to a larger number of vesicles adsorbed on the surface) for the measurement at 25 °C indicates that a higher concentration and a stronger deformation of vesicles are required in mixed lipid phases before vesicle rupture takes place. In addition to the thermal activation of the vesicles, we believe that the lipid phase plays a critical role. Previously it has been described that the mean curvature bending modulus of the solid phase is considerably higher than that of the liquid phase.[47] Furthermore, the cholesterol of the lipid compositions preferably locates at the phase boundary and accommodates a certain level of vesicle deformation.[32] As a result, a larger intervesicular stress is required for the ruptures of the vesicles within the mixed lipid phases.

3.2. Melittin–Membrane Interaction under QCM-D Monitoring. In addition to the mass and viscoelasticity, the f and D values of different overtones obtained from a QCM-D measurement can provide three-dimensional information of the film on the sensor surface.[3,26] The penetration depth of the harmonic wave is inversely proportional to its frequency. Therefore, the measurement at higher overtones is surface sensitive while that at lower overtones probe deep inside of the film. The overtone effect during SLB formation is shown in the left of Figure 3. At both 25 and 50 °C, the traces of different harmonics spread out along with the adsorption of vesicles, while after vesicle rupture and SLB formation, all harmonics overlap (Stage A), indicating that membranes with the homogeneity in the direction normal to the surface have been obtained.

After the SLB formation, melittin solution was injected *in situ* (right in Figure 3), to examine the dynamic interaction process

dx.doi.org/10.1021/jp305141r | J. Phys. Chem. B 2012, 116, 9432–9438

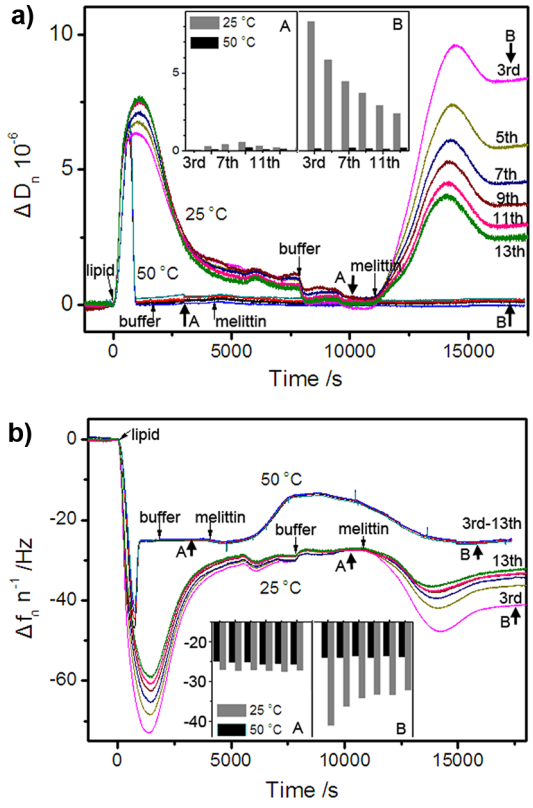

Figure 3. Real-time QCM-D responses, ΔD and Δf, during the vesicle deposition and subsequent membrane-melittin interaction processes at different temperatures (25 and 50 °C). The nonbold arrows (marked with lipid, buffer, or melittin) are indicating the injection of certain solutions, while the bold ones (marked with A and B) refer to certain stages before and after the melittin acting process. Inset: overtone effect showing the changes in both ΔD and Δf, before (stage A) and after (stage B) the melittin actions.

of melittin with membranes of different states. For the SLB in liquid phase at 50 °C, with the addition of melittin, the value of Δf increased gradually after a slight decrease, followed by another obvious decrease and finally to a steady state of −25.9 ± 0.2 Hz, slightly lower than that without peptide (−25.0 ± 0.2 Hz). The frequency variations measured by all overtones were the same. Meanwhile, the dissipation responses at all overtones almost remained zero during the melittin−membrane interaction process. These overtone-phenomena indicate a process which has the same structure characteristics across the whole membrane, consistent with a trans-membrane behavior without significant disturbance to the vertical homogeneity of the membrane.[3,26] In this case, the initial variations in Δf (corresponding to a little disturbance in ΔD) suggest the slight upload of melittin on the membrane (i.e., tiny decrease in Δf), and consequently the increase in frequency indicates a loss of the whole mass on the sensor surface. Such a loss may be induced by the trans-membrane behaviors including solubilization (e.g., micellization) and removal of lipid-melittin complexes due to melittin insertion, followed by the pore formation across the membrane. Here, a thinning of bilayer with expelling the swollen water from the membrane due to the adsorption of melittin can also possibly happen during this process. Then the continuously added peptides from the flow-through system keep adsorbing, probably to the previously inserted ones, and such an adsorption becomes the primary process shown as a frequency decrease in the QCM measurement. The adsorption dominated process continues until reaching a threshold value of the melittin content in the membrane, where saturation or dynamic equilibrium is reached. The final mass on the sensor chip surface (stage B) is comparable to the initial state (shown as a bar chart in Figure 3, inset), confirming that no membrane disintegration occurs and the primary action takes place during the pore formation. However, at 25 °C, the membrane−peptide interaction behaved differently. Adding melittin induced a decrease of Δf immediately, followed by an increase, corresponding to the increase and decrease in ΔD, respectively, until reaching a steady state. At the same time, both the frequency and dissipation responses measured at different overtones deviated significantly from each other. It is noted that the order of the harmonics for dissipation during the disruption caused by melittin is in the reverse order than that of the vesicle prerupture process. This would emphasize the difference in structure distribution within the membrane for the two cases. After the interaction process, the frequency response reached a final value of −45 (−45 to −35, from the 3rd to 13th overtone) ± 0.5 Hz, and the dissipation response was 9 (9−3, respectively) ± 0.5 × 10^{-6}, much larger than those prior to the interaction (depicted as a bar chart in Figure 3 inset for clarity). The initial increases and deviations in Δf (absolute value) and ΔD distinctly represent a melittin adsorption process, and subsequently, the decreases and continued deviations suggest a vertical inhomogeneous mass removal dominated process. Especially, the final mass on the sensor chip surface is more than the initial state. On the basis of these results, we can propose a surface binding followed by an asymmetrical disruption dominated mechanism in the membrane.

In context of the literature models of membrane disturbance,[11−13] a carpet mechanism is adopted and the melittin activities on membranes with different phases are illustrated in Figure 4. For a liquid phase, membrane lysis takes

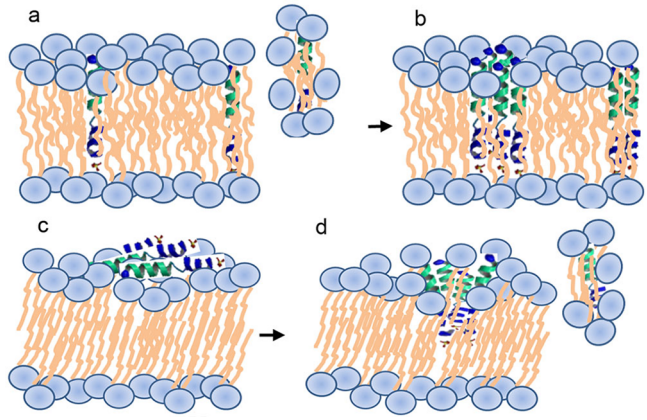

Figure 4. Schematic representation of the interaction mechanism between melittin and SLB with liquid (a−b) or solid phase (c−d). Mechanisms include: transmembrane insertion of melittin with membrane lysis (a) and further melittin incorporation (b), carpet association (c) and subsequent partial insertion with asymmetrical membrane disruption (d).

place immediately after the upload of melittin *via* transmembrane peptide insertion and pore formation, along with the solubilization and removal of peptide−lipid complexes which leads to the mass decrease of the whole membrane (a). With the further injection of melittin, the peptide incorporation

dx.doi.org/10.1021/jp305141r | J. Phys. Chem. B 2012, 116, 9432−9438

behavior proceeds and becomes the primary process, along with the mass increase, until reaching saturation (b). In this condition, no distinct critical peptide-to-lipid ratio effect, which is the case of a carpet mechanism, is observed prior to melittin insertion. However, in the solid-phase domain where the lipid tails are closely packed (c and d), the threshold peptide-to-lipid ratio effect becomes more obvious. The initially injected melittin molecules adsorb on the solid membrane surface (c), due to the less steric repulsion contributed from the less fluid bilayers compared to the more fluid and fluctuating bilayers.[32] However, above a threshold value of peptide-to-lipid ratio, mass removal process *via* partial peptide insertion and asymmetrical membrane disruption (and/or buckling) (d) becomes predominant, leading to the formation of a highly nonuniform surface structure. Besides the temperature effect on peptide activity, the state of the membrane is supposed to play a critical role in determining the melittin−membrane interaction.

3.3. Simulation Results. To further understand the molecular mechanism of melittin−membrane interactions, a computer simulation method was introduced. The detailed insertion process of a single melittin into the lipid bilayer is obtained by DPD simulations and shown in Figure 5. At the beginning,

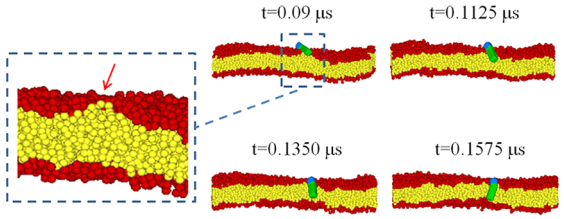

Figure 5. Cross-sectional snapshots during the insertion process of melittin into a lipid bilayer. Dotted line box shows the enlarged figure of the region of the membrane where melittin acts (red arrow, melittin is not shown for clarity).

melittin is located horizontally to the surface of the membrane. It is found that the peptide reorients from horizontal to vertical to the bilayer rapidly during its interaction with the lipid molecules. It can be observed that the key step of this reorientation is the formation of a defect on the surface of the bilayer. Under the disturbance of the adsorbed melittin (Figure 5, dotted line box), the heads of lipids are disrupted locally and the tails reorient somewhat during their interactions with the hydrophobic surface of melittin. Such a disturbance on the bilayer in turn facilitates the insertion of melittin into the membrane. This mechanism might also help explain the experimental result that the insertion of peptide into a membrane in liquid phase takes place much sooner and easier than in a solid one.

However, we found that in our simulations, not all the melittin on the surface can insert into the bilayer (cf. Supporting Information, movie S1). To acquire the insertion custom of melittin into membrane, systems of melittin with different relative number densities to lipid are proposed and the melittin action process is further explored. To quantitatively evaluate the insertion capacity of melittin into the bilayer, a parameter P, defined as the percentage of the melittin inserted, is obtained from the statistical result of the multisimulations as

$$P\ (\%) = \frac{\sum_i^{N_s} n_{pi}}{\sum_i^{N_s} n_p} 100$$

where n_p is the total number of melittin under concerned in simulations and n_{pi} denotes the number of those inserted. N_s is the independent simulation times. It is shown in Figure 6 that

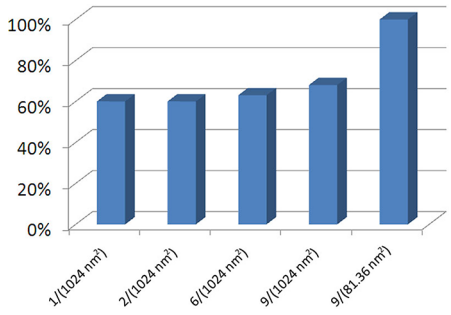

Figure 6. Number-density dependence of the insertion capacity (P) of melittin. The result is obtained from an average of five independent simulations.

the insertion capacity of melittin increases with its number density on the surface [i.e., from n_p/area = 1/1024 to 9/(1024 nm^2), P increases from ∼60% to ∼68%]. When the number density is high enough [∼9/(81 nm^2)], almost all the melittin in simulations would insert into the membrane.

On the other hand, the local number density of melittin (i.e., the local peptide-to-lipid ratio) also plays an important role in determining the peptide insertion. For example, with a fixed membrane area and a similar amount of melittin (*e.g.*, n_p = 9), the insertion process would be rather facilitated if all the peptides are located crowdedly in a confined region (i.e., with a higher local number density) compared to the case distributed uniformly across the whole surface. This result can be clearly observed by the comparison between movies S1 and S2 in the Supporting Information.

The above results are expected to provide an attractive insight into the conventional carpet mechanism. As shown in Figure 7a and movie S2, melittin with a higher local

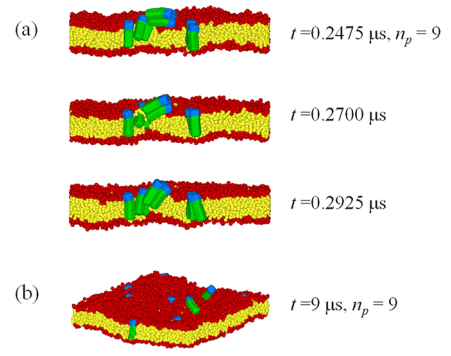

Figure 7. Snapshots during the insertion of melittin (n_p = 9) into a lipid bilayer. At the beginning, the melittin molecules are located densely in a small region of 81.36 nm^2 (a) or distributed evenly across the whole surface (b). The snapshots are captured from the supplementary movies S2 and S1, respectively.

concentration acts in a significantly different method compared to that with a lower local concentration (Figure 7b and movie S1). The insertion of melittin probably takes place by those who have already inserted, due to the variation of packing state of the surrounding lipids.[35] Furthermore, two or more melittin molecules frequently bind together before/during

dx.doi.org/10.1021/jp305141r | J. Phys. Chem. B 2012, 116, 9432−9438

inserting into the membrane. This binding behavior might reduce the contact of the hydrophobic region of melittin with the aqueous solvent and also enhance the perturbance from the intruder to the surrounding lipids to some extent. Such a cooperation effect might be the reason that a carpet mechanism is adopted during the peptide−membrane interaction process. On the contrary, with a locally lower melittin concentration (Figure 6), such as the case of melittin being distributed uniformly across the surface, not all the peptides inserted the membrane even after a long time (i.e., t = 9 μs, Figure 7b).

4. CONCLUSIONS

We have combined the methods of QCM-D experiment and computer simulation to explore the interaction mechanism of melittin and membrane. Lipid phase plays an important role in determining the melittin−membrane interaction process. A vertical transmembrane peptide insertion takes place right after the upload of melittin onto a liquid bilayer, while for a solid membrane, a "carpet" mechanism is adopted. Melittin associates with the membrane followed by a partial peptide insertion and an asymmetrical membrane disruption. The detailed insertion process of melittin into the membrane based on computer simulations could explain the difference. The simulation results demonstrate that upon the adsorption of the peptide, the disturbance on the lipid especially the reorientation of lipid tails, which is apt to occur in a liquid phase, in turn facilitates the insertion of melittin into the membrane. At the same time, the dependence of the insertion capacity of melittin on the local peptide number concentration was observed. With a higher peptide-to-lipid ratio (even only in a local region on the surface), a cooperation effect in neighboring peptides on insertion takes place, consistent with the "carpet" phenomena in experiments.

■ ASSOCIATED CONTENT

Supporting Information

Movies S1 and S2 showing the insertion process of melittin (n_p = 9) into the membrane in simulations. This material is available free of charge via the Internet at http://pubs.acs.org.

■ AUTHOR INFORMATION

Corresponding Author

*Tel/Fax: 86 512 65220239. E-mail: yuanbing@suda.edu.cn (B.Y.). Tel./Fax: 86 25 83592900. E-mail: myqiang@nju.edu.cn (Y.M.).

Notes

The authors declare no competing financial interest.

■ ACKNOWLEDGMENTS

This work was financially supported by the National Science Foundation of China (Nos. 91027040, 10974080, 21106114, and 11104192) and the National Basic Research Program of China (No. 2012CB821500). B. Yuan thanks the China Postdoctoral Science Foundation (No. 201104557). K. Yang thanks the support of the Key Project of Chinese Ministry of Education (No. 210208) and the Applied Basic Research Program (No. 2010CD091) of Yunnan Province of China.

■ REFERENCES

(1) Brogden, K. A. *Nat. Rev. Microbiol.* **2005**, *3*, 238−250.
(2) Hancock, R. E. W.; Sahl, H. G. *Nat. Biotechnol.* **2006**, *24*, 1551−1557.
(3) McCubbin, G. A.; Praporski, S.; Piantavigna, S.; Knappe, D.; Hoffmann, R.; Bowie, J. H.; Separovic, F.; Martin, L. L. *Eur. Biophys. J.* **2011**, *40*, 437−446.
(4) Malmsten, M.; Stromstedt, A. A.; Ringstad, L.; Schmidtchen, A. *Curr. Opin. Colloid Interface Sci.* **2010**, *15*, 467−478.
(5) Gee, M. L.; Rapson, A. C.; Hossain, M. A.; Wade, J. D.; Nice, E. C.; Smith, T. A.; Clayton, A. H. A. *Biophys. J.* **2011**, *100*, 1353−1361.
(6) Chattopadhyay, A.; Raghuraman, H. *Biosci. Rep.* **2007**, *27*, 189−223.
(7) Pasha, S.; Joshi, S.; Bisht, G. S.; Rawat, D. S.; Kumar, A.; Kumar, R.; Maiti, S. *Biochim. Biophys. Acta, Biomembr.* **2010**, *1798*, 1864−1875.
(8) Fantner, G. E.; Barbero, R. J.; Gray, D. S.; Belcher, A. M. *Nat. Nanotechnol.* **2010**, *5*, 280−285.
(9) Stankowski, S.; Pawlak, M.; Kaisheva, E.; Robert, C. H.; Schwarz, G. *Biochim. Biophys. Acta* **1991**, *1069*, 77−86.
(10) Guidelli, R.; Becucci, L.; Leon, R. R.; Moncelli, M. R.; Rovero, P. *Langmuir* **2006**, *22*, 6644−6650.
(11) Shai, Y. *Biochim. Biophys. Acta* **1999**, *1462*, 55−70.
(12) Huang, H. W. *Biochemistry* **2000**, *39*, 8347−8352.
(13) Gheorghiu, E.; Olaru, A.; Gheorghiu, M.; David, S.; Wohland, T. *J. Phys. Chem. B* **2009**, *113*, 14369−14380.
(14) Poolman, B.; van den Bogaart, G.; Guzman, J. V.; Mika, J. T. *J. Biol. Chem.* **2008**, *283*, 33854−33857.
(15) Mihajlovic, M.; Lazaridis, T. *Biochim. Biophys. Acta, Biomembr.* **2010**, *1798*, 1485−1493.
(16) Hristova, K.; Dempsey, C. E.; White, S. H. *Biophys. J.* **2001**, *80*, 801−811.
(17) Swann, M. J.; Popplewell, J. F.; Freeman, N. J.; McDonnell, C.; Ford, R. C. *Biochim. Biophys. Acta, Biomembr.* **2007**, *1768*, 13−20.
(18) Chattopadhyay, A.; Raghuraman, H. *Biophys. J.* **2004**, *87*, 2419−2432.
(19) Wessman, P.; Stromstedt, A. A.; Malmsten, M.; Edwards, K. *Biophys. J.* **2008**, *95*, 4324−4336.
(20) Chattopadhyay, A.; Raghuraman, H. *Biophys. J.* **2007**, *92*, 1271−1283.
(21) Lundquist, A.; Wessman, P.; Rennie, A. R.; Edwards, K. *Biochim. Biophys. Acta, Biomembr.* **2008**, *1778*, 2210−2216.
(22) Tang, Y.; Wang, Z.; Xiao, J.; Yang, S.; Wang, Y.; Tong, P. *J. Phys. Chem. B* **2009**, *113*, 14925−14933.
(23) Gheorghiu, M.; Olaru, A.; Tar, A.; Polonschii, C.; Gheorghiu, E. *Biosens. Bioelectron.* **2009**, *24*, 3517−3523.
(24) Rapson, A. C.; Hossain, M. A.; Wade, J. D.; Nice, E. C.; Smith, T. A.; Clayton, A. H. A.; Gee, M. L. *Biophys. J.* **2011**, *100*, 1353−1361.
(25) Ding, B.; Chen, Z. *J. Phys. Chem. B* **2012**, *116*, 2545−2552.
(26) Mechler, A.; Praporski, S.; Atmuri, K.; Boland, M.; Separovic, F.; Martin, L. L. *Biophys. J.* **2007**, *93*, 3907−3916.
(27) Seantier, B.; Breffa, C.; Felix, O.; Decher, G. *J. Phys. Chem. B* **2009**, *109*, 21755−21765.
(28) Yuan, B.; Zhu, T.; Zhang, Z.; Jiang, Z.; Ma, Y. *J. Mater. Chem.* **2011**, *21*, 3471−3476.
(29) Hook, F.; Kasemo, B.; Nylander, T.; Fant, C.; Sott, K.; Elwing, H. *Anal. Chem.* **2001**, *73*, 5796−5804.
(30) Woo, H.-J.; Wallqvist, A. *J. Phys. Chem. B* **2011**, *115*, 8122−8129.
(31) Yang, K.; Ma, Y. Q. *Nat. Nanotechnol.* **2010**, *5*, 579−583.
(32) Sundh, M.; Svedhem, S.; Sutherland, D. S. *Phys. Chem. Chem. Phys.* **2010**, *12*, 453−460.
(33) Hoogerbrugge, P. J.; Koelman, J. M. V. A. *Europhys. Lett.* **1992**, *19*, 155−160.
(34) Espanol, P.; Warren, P. *Europhys. Lett.* **1995**, *30*, 191−196.
(35) Venturoli, M.; Smit, B.; Sperotto, M. M. *Biophys. J.* **2005**, *88*, 1778−1798.
(36) Schmidt, U.; Guigas, G.; Weiss, M. *Phys. Rev. Lett.* **2008**, *101*, 128104.
(37) de Meyer, F. J.-M.; Rodgers, J. M.; Willems, T. F.; Smit, B. *Biophys. J.* **2010**, *99*, 3629−3638.
(38) Reynwar, B. J.; Illya, G.; Harmandaris, V. A.; Muller, M. M.; Kremer, K.; Deserno, M. *Nature* **2007**, *447*, 461−464.

(39) Ding, H. M.; Tian, W. D.; Ma, Y. Q. *ACS Nano* **2012**, *6*, 1230−1238.
(40) Ding, H. M.; Ma, Y. Q. *Biomaterials* **2012**, *33*, 5798−5802.
(41) Raghuraman, H.; Chattopadhyay, A. *Biosci. Rep.* **2007**, *27*, 189−223.
(42) Bao, D. C.; Hang, Q. G.; Liu, X. D.; Ma, X. J.; Yuan, Q. *Acta Phys., Chim. Sin.* **2004**, *20*, 178−181.
(43) Li, D. W.; Liu, X. Y. *J. Chem. Phys.* **2005**, *122*, 174909.
(44) Hong, B. B.; Qiu, F.; Zhang, H. D.; Yang, Y. L. *J. Phys. Chem. B* **2007**, *111*, 5837−5849.
(45) Yue, T.; Li, S.; Zhang, X.; Wang, W. *Soft Matter* **2010**, *6*, 6109−6118.
(46) Rodahl, M.; Hook, F.; Fredriksson, C.; Keller, C. A.; Krozer, A.; Brzezinski, P.; Voinova, M.; Kasemo, B. *Faraday Discuss.* **1997**, *107*, 229−246.
(47) Baumgart, T.; Das, S.; Webb, W. W.; Jenkins, J. T. *Biophys. J.* **2005**, *89*, 1067−1080.